A dayside auroral energy deposition case study using the Polar Ultraviolet Imager

M. Brittnacher,[1] R. Elsen,[1] G. Parks,[1] L. Chen[1] G. Germany,[2] and J. Spann[3]

Abstract. In this letter, we report preliminary results from a study of dayside auroral energy deposition during quiet times using global auroral images acquired by the Ultraviolet Imager experiment on the Polar spacecraft. Solar wind plasma and interplanetary magnetic field measurements from the Wind spacecraft and K_P values were used to characterize the state of the magnetosphere. The auroral oval was observed for a two-hour period in spring and summer during relatively quiet times ($K_P \simeq 0$ to 1). We find that, although the night-side energy deposition rate varied by an order of magnitude to as low as 1×10^{16} erg s^{-1} (1 gigawatt), the dayside was much less variable and remained between 4 and 10×10^{16} erg s^{-1}.

Introduction

Global measurement of the spatial and temporal variation of auroral energy deposition in conjunction with solar wind and magnetospheric monitoring during the International Solar Terrestrial Physics campaign is an important component in the study of solar wind–geomagnetic field–ionospheric interactions. Since some of the processes involved in energy transport to the ionosphere have timescales on the order of a few minutes and affect a large portion of the auroral region, high time resolution monitoring of the global aurora is required. Previous estimates of energy deposition over a large fraction of the nightside auroral oval have been derived from ISIS-2 [*Murphree and Anger*, 1978] and Dynamics Explorer-1 [*Rees et al.*, 1988] spin-scan photometer images acquired at ultraviolet wavelengths. More recently, averaging of particle measurements from many low-altitude satellite passes have provided global estimates of auroral energy deposition [*Evans*, 1987].

The Ultraviolet Imager (UVI) experiment [*Torr et al.*, 1995] on the Polar spacecraft enables the study of global auroral energy deposition at a time resolution on the order of minutes over several hours at a time. The UVI camera is mounted on a despun platform whose pointing direction is adjusted periodically to maximize viewing of the entire oval. A unique feature of the UVI camera is the newly developed narrow-band,

[1] Geophysics Program, University of Washington, Seattle, WA

[2] University of Alabama, Huntsville, AL

[3] NASA Marshall Space Flight Center, Huntsville, AL

far-ultraviolet filters. The Lyman-Birge-Hopfield 140–160 nm short wavelength (LBHs) and 160–180 nm long wavelength (LBHl) filters are designed to separate the LBH band observations into two sections divided by a sharp decline in O_2 absorption. By separately measuring emissions in the longer and shorter portions of the LBH band, the energy flux and characteristic energy of the precipitating electrons can be inferred with the aid of auroral transport models [*Germany et al.*, 1994a; *Lummerzheim et al.*, 1997]. The instantaneous ionospheric conductivity can also be derived from these measurements [*Germany et al.*, 1994b]. These data provide useful inputs to models of the high-latitude ionosphere, such as AMIE that will be used in the MAMI (Modeling of the Atmosphere–Magnetosphere–Ionosphere) investigation [*Rees et al.*, 1995].

In this preliminary case study we analyzed a series of six UVI images during relatively quiet times ($K_P \simeq 0$ to 1) on each of two days in the northern hemisphere spring and summer. We have created energy deposition maps of the global aurora to study the energy input to distinct regions of the ionosphere. Observations of solar wind plasma by the SWE experiment [*Ogilvie et al.*, 1995] and the interplanetary magnetic field (IMF) by the MFI experiment [*Lepping et al.*, 1995] on the Wind spacecraft monitored solar wind conditions.

Observations

A two-hour period on April 7, 1996 when the Polar spacecraft was near apogee over the northern hemisphere and K_P was 0° was selected for the first study. Six images acquired at 0600, 0618, 0643, 0737, 0749, and 0801 UT with the LBHl filter were chosen. Although LBHl images were available every six minutes at this time, higher time resolution was not considered necessary during this quiet period. Only one image from each day will be used to illustrate the procedure. The image acquired at 0737 UT is plotted in geographic coordinates in Figure 1a. Local noon is toward the upper right side of the image. The linear color scale indicates the photon flux (photons cm^{-2} s^{-1}) collected in the instrument aperture. To convert photon flux to surface brightness in Rayleighs for each pixel multiply by $4\pi/(\Omega\,10^6) \approx 30.17$, where Ω is the solid angle subtended by a single pixel (4.17×10^{-7} sr) [*Torr et al.*, 1995]. The one count level at this time was about 17 Rayleighs, where "counts" refers to electrons generated at the photocathode in the UVI detector. The brightest emissions in the image (red) are about 600 Rayleighs. The intensity recorded for the dayside auroral oval includes sunlit airglow. The edge of the 8° field of view
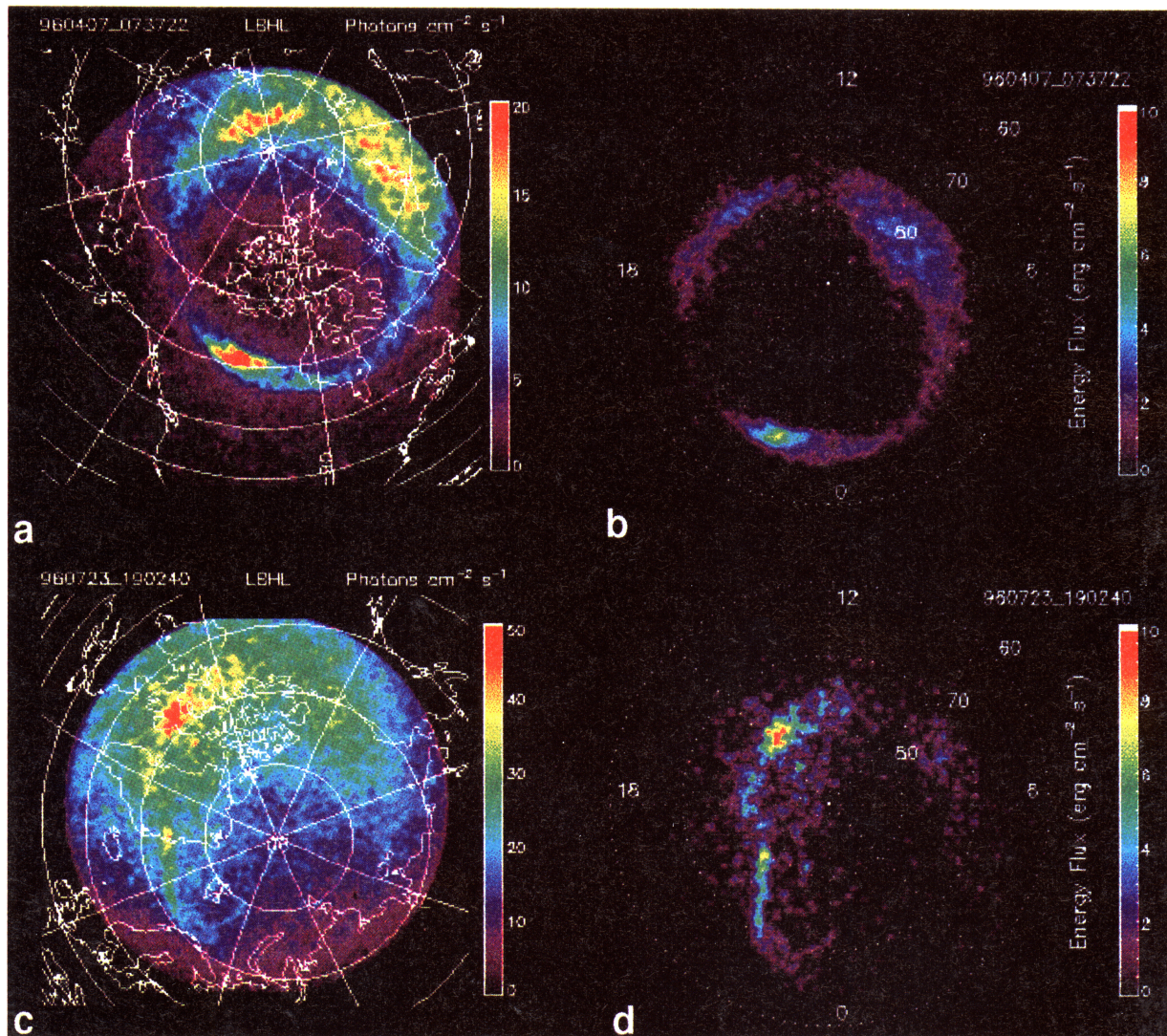
Figure 1. The auroral oval at 0737 UT on April 7, 1996 in (a) geographic coordinates (overlaid with 10° latitude and 45° longitude gridlines) and (b) transformed to MLT coordinates with the dayglow removed. The auroral oval at 1902 UT on July 23, 1996 in (c) geographic coordinates and (d) MLT coordinates with the dayglow removed.

appears as a sharp semi-circular edge of the bright colors along the top and right edge of the figure.

The 0737 UT image with the dayglow removed is plotted in magnetic local time (MLT) using a tilted dipole coordinate system (Figure 1b). The dayglow is modeled as a smooth, monotonically decreasing function of solar zenith angle directly from the image data outside of the auroral region. The error associated with the final photon flux attributed to auroral electron precipitation is about 20% based on the statistical noise in the images. The linear color scale represents the energy flux of the precipitating electrons in units of erg cm^{-2} s^{-1}. The conversion from surface brightness to energy flux is discussed below. The average energy deposition rate in the ionosphere was about 3 erg cm^{-2} s^{-1} over the entire oval.

The oval and polar cap boundary in Figure 1b are approximately circular and are defined by an energy flux greater than 0.5 erg cm^{-2} s^{-1}. The actual boundary of

the oval may occur at a different latitude from that observed if the emissions are below the sensitivity of the UVI camera. Although K_P was 0° during this period, some activity on the nightside was observed. A localized region of intense precipitation in the pre-midnight sector faded gradually from 0600 UT and is still seen in Figure 1b. The solar wind dynamic pressure was very steady during the study interval at $\sim$ 1.7 nanopascals (nPa). IMF magnitude was also relatively steady and quite low, never exceeding 3 nT. IMF B_y was the dominant component ($\geq$ 2 nT) for the entire study period, while IMF B_z rarely exceeded 1 nT in magnitude. Using a 30-minute solar wind propagation time from Wind indicates IMF B_z was weakly southward on average (-0.5 nT) for the half hour period surrounding the 0737 image. These solar wind conditions are consistent with the quiescent state of the magnetosphere during the study interval.

A second set of images was selected from the July 23

apogee pass when K_P was 1^+ and discrete arc activity was more prevalent. The six images acquired at 1747, 1806, 1825, 1844, 1902, and 1921 UT were obtained using the LBHl filter. The image at 1902 UT is plotted in geographic coordinates in Figure 1c. The dayside is toward the top of the image and the dayglow extends across the entire oval. Earth's dipole at this time was highly tilted at about 28°. Multiple arcs were seen on the duskside and some of these developed into transpolar arcs. A localized hot spot in the high-latitude, 14-MLT region indicates dynamic activity on the dayside apart from substorms or other intense precipitation on the nightside.

The 1902 UT image with the dayglow removed is plotted in magnetic latitude and local time (Figure 1d). After dayglow removal the enhancement at 14 MLT remains the most prominent feature with an energy flux exceeding 10 erg cm^{-2} s^{-1} for a forty-minute period (1900 to 1940 UT). The bright arc bands on the duskside lie within the conventional oval. The polar cap, although not well defined on the dawnside, is much smaller than in the April 7, 0737 UT image, reminiscent of the teardrop-shaped polar cap previously reported by *Lundin et al.* [1991]. While the afternoon dominates dayside emissions on July 23, it is only half that in the morning sector on April 7. Solar wind conditions measured at Wind were very similar to those on April 7 but not quite as steady. Dynamic pressure was again low, but gradually dropped from 1.5 to 1.0 nPa. IMF magnitude was again below 3 nT for almost the entire study period, most of the time dominated by positive B_y near 2 nT with a weakly negative B_z (−0.5 nT).

Energy Deposition

One-dimensional transport models that calculate column integrated intensities for incident auroral electrons
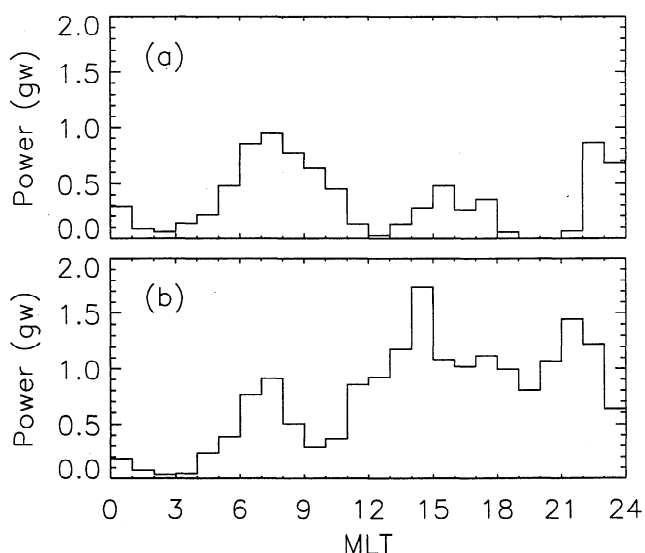
Figure 2. The total energy deposited between 60° and 90° N latitude as a function of the MLT hour angle, measured in gigawatts $(10^{16}\text{erg s}^{-1})$ and plotted at one-hour resolution, for (a) April 7, 1996 and (b) July 23, 1996 at the same times as in Figure 1.
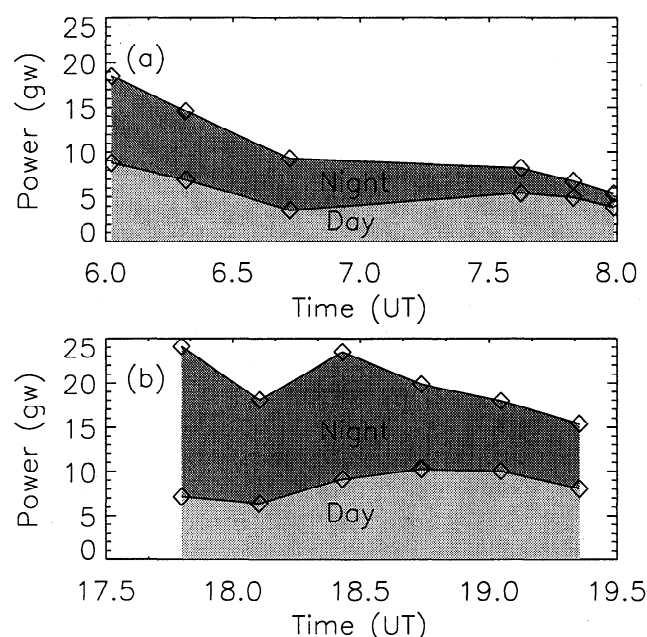
Figure 3. The dayside and nightside energy in gigawatts $(10^{16}\text{erg s}^{-1})$ for (a) April 7, 1996 and (b) July 23, 1996. The diamonds show the times at which the images were acquired. The lower (upper) shaded region represents the dayside (nightside) energy. The top line is the total precipitation energy over the auroral oval.

[*Germany et al.*, 1994a; *Lummerzheim et al.*, 1997] determine a proportionality relation between surface brightness (convolved with the bandpass of the LBHl filter) and auroral electron energy flux of approximately 110 Rayleighs per erg cm^{-2} s^{-1}. Seasonal and latitudinal variations were not taken into account in the calculation of the brightness to energy flux relationship since the accuracy of the dayglow removal from the images was not great enough to justify higher order corrections to the model atmosphere. The one count level in the UVI data translates into a minimum detectable energy flux of about 0.2 erg cm^{-2} s^{-1}.

The total energy deposition rate in each MLT hour angle between 60° and 90° N latitude for the study images was calculated by integration of the energy flux over the total area in the (pie-shaped) hour angle sector and is plotted for the 0737 UT image on April 7 (Figure 2a). Three distinct regions of precipitation are seen—in the morning, afternoon, and duskside sectors. Energy deposition is mostly in a single structure extending from 4 to 12 MLT. The dip at noon where the energy deposition rate drops below 1×10^{16} erg s^{-1} (1 gigawatt) was observed in all energy plots in this study period (not shown), and at 0643 UT extends from 10 to 15 MLT.

The dayside, nightside, and total oval energy deposition rates for the six April 7 images are shown in Figure 3a. The diamonds represent the times at which the UVI images were acquired. The dayside was defined to begin at 0600 MLT and end at 1800 MLT, an arbitrary division that does not account for the different source regions of the precipitating particles or factors (e.g., IMF

conditions) that can shift auroral features with respect to local time. The energy deposition is underestimated for the 0643, 0749, and 0802 UT images due to incomplete viewing of the dayside oval. The dayside energy deposition varied from 4 to 9×10^{16} erg s^{-1} whereas the nightside rate varied between 1 and 10×10^{16} erg s^{-1}. Thus, although the nightside energy deposition varied by an order of magnitude to as low as 1×10^{16} erg s^{-1}, the dayside varied by about a factor of 2 for this data set. If the (underestimated) energy rate in Figure 3a were corrected for the incomplete viewing, it is expected that the dayside energy value would be even less variable for that two-hour period.

The energy for each hour angle for the 1902 UT image on July 23 (Figure 2b) shows three regions of energy deposition that may map to three different regions of the magnetosphere. Energy deposition in the afternoon is greater than in the morning and the enhancement at 14 MLT is clearly seen. The day and night energy deposition rate for the July 23 study period (Figure 3b) varied between 6 and 10×10^{16} erg s^{-1}, similar to the April 7 values. The nightside varied over a greater range, from 7 to 17×10^{16} erg s^{-1}.

Discussion

This case study is the first step toward using the global energy deposition measurements derived from UVI images and the solar wind plasma and IMF measurements from the Wind spacecraft to study the problem of the coupling of energy from the solar wind to the dayside ionosphere. Our main conclusion is that the dayside emissions appear to vary less than the nightside during quiet times. The lowest value for the global energy deposition in this study of about 5×10^{16} erg s^{-1} is similar to the estimated lower bound of 4×10^{16} erg s^{-1} obtained by *Murphree and Anger* [1978] from ISIS-2 imager data. Future studies will include more active times to determine quantitatively how dayside energy deposition is influenced by nightside activity during more active times and what fraction of the global auroral energy deposition occurs on the dayside as a function of activity level.

Since the dayside energy deposition in the quiet oval was approximately the same for both the spring and summer study periods, further study is called for to determine whether this is typical or whether there are seasonal variations in the average energy deposition on the dayside due to the solar enhancement of the local conductivity as reported by *Newell et al.* [1996].

This study has focused on the use of UVI images to obtain global auroral energy deposition measurements which can be obtained with single images. Future studies will use the capability of the narrow-band filters for two consecutive images to derive the characteristic energy of the precipitating electrons to aid in the determination of the source population, and will also determine the ionospheric conductivity from electron/ion pair pro-

duction calculated from energy deposition and characteristic energy measurements [*Germany et al.*, 1994a, 1994b]. Finally, detailed characterization of the source regions by *in situ* spacecraft along with global auroral energy deposition measurements would provide a significant advance in the understanding of solar wind-magnetospheric coupling processes.

References

Evans, D. S., Global statistical patterns of auroral phenomena, in *Quantitative Modeling of Magnetosphere-Ionosphere Coupling Processes*, ed. by Y. Kamide and R. A. Wolf, Kyoto, 1987.

Germany, G. A., M. R. Torr, D. G. Torr, and P. G. Richards, Use of FUV auroral emissions as diagnostic indicators, *J. Geophys. Res.*, *99*, 383, 1994a.

Germany, G. A., D. G. Torr, P. G. Richards, M. R. Torr, and S. John, Determination of ionospheric conductivities from FUV auroral emissions, *J. Geophys. Res.*, *99*, 23297, 1994b.

Lepping, R. P., et al., The Wind magnetic field investigation, *Space Sci. Rev.*, *71*, 207, 1995.

Lummerzheim, D., M. Brittnacher, D. Evans, G. A. Germany, G. K. Parks, and J. F. Spann, High time resolution study of the hemispheric energy flux carried by energetic electrons in the ionosphere during the May 19/20, 1996 auroral activity, *Geophys. Res. Lett.*, in press, 1997.

Lundin, R., L. Eliasson, and J. S. Murphree, The quiet-time aurora and the magnetospheric configuration, in *Auroral Physics*, ed. C.-I. Meng, M. J. Rycroft, and L. A. Frank, Cambridge University Press, 1991.

Murphree, J. S., and C. D. Anger, Instantaneous auroral particle energy deposition as determined by optical emissions, *Geophys. Res. Lett.*, *5*, 551, 1978.

Newell, P. T., C.-I. Meng, and K. M. Lyons, Suppression of discrete aurorae by sunlight, *Nature*, *381*, 766, 1996.

Ogilvie, K. W., et al., SWE, a comprehensive plasma instrument for the Wind spacecraft, *Space Sci. Rev.*, *71*, 55, 1995.

Rees, M. H., D. Lummerzheim, R. G. Roble, J. D. Winningham, J. D. Craven, and L. A. Frank, Auroral energy deposition rate, characteristic electron energy, and ionospheric parameters derived from Dynamics Explorer 1 images, *J. Geophys. Res.*, *93*, 12841, 1988.

Rees, M. H., D. Lummerzheim, and R. G. Roble, Modeling of the atmosphere-magnetosphere-ionosphere system MAMI, *Space Sci. Rev.*, *71*, 691, 1995.

Torr, M. R., et al., A far ultraviolet imager for the international solar-terrestrial physics mission, *Space Sci. Rev.*, *71*, 329, 1995.

M. Brittnacher, L. Chen, R. Elsen, G. Parks, Geophysics Program, Box 351650, University of Washington, Seattle, WA 98195 (e-mail: britt@geophys.washington.edu).

G. Germany, Center for Space Plasma and Aeronomic Research, University of Alabama, Huntsville, AL 35899.

J. Spann, Space Sciences Laboratory, NASA Marshall Space Flight Center, Huntsville, AL 35812.